NASA/TM—1999-209178

Investigation of Atomic Oxygen Erosion of Polyimide Kapton H Exposed to a Plasma Asher Environment

Aaron Snyder
Glenn Research Center, Cleveland, Ohio

Prepared for the
44th International SAMPE Symposium and Exhibit
sponsored by the Society for the Advancement of Material and Process Engineering
Long Beach, California, May 23–27, 1999

National Aeronautics and
Space Administration

Glenn Research Center

May 1999

This report is a formal draft or working paper, intended to solicit comments and ideas from a technical peer group.

Available from

NASA Center for Aerospace Information
7121 Standard Drive
Hanover, MD 21076
Price Code: A03

National Technical Information Service
5285 Port Royal Road
Springfield, VA 22100
Price Code: A03

INVESTIGATION OF ATOMIC OXYGEN EROSION OF POLYIMIDE KAPTON H EXPOSED TO A PLASMA ASHER ENVIRONMENT

Aaron Snyder
National Aeronautics and Space Administration
Glenn Research Center
Cleveland, Ohio 44135

ABSTRACT

Experimental results are presented on the erosion characteristics of the polyimide Kapton H, which serves as a blanket material in solar arrays. This polymer has a number of characteristics that make it a suitable choice for both terrestrial and space applications. In this paper attention is focused on the durability of protected Kapton when exposed to atomic oxygen (AO) in a plasma asher. A strip of 0.025-mm thick Kapton film, coated on both sides with SiO_2, was studied during a 1306 hour exposure. The erosion, located at defect sites in the protective coating and measured optically, is described in terms of volume loss as a function of AO fluence. Three simple geometric profiles are used to generate a useful array of cavity shapes to model erosion evolution. These models connect the volume erosion rate to the observed lateral expansion of the developing cavities via their diameters, measured adjacent to the upper and lower protective film, and fitted by least-squares regression to simple power law functions of fluence. The rationale for the choice of models is discussed. It was found that lateral growth in cavity size evolves less than linearly with fluence.

KEY WORDS: Atomic Oxygen (AO), Protective Coatings, Undercutting

1. INTRODUCTION

Understanding the behavior of polymeric materials when exposed to the low-Earth-orbit environment is important in predicting performance characteristics such as in-space durability. Experimental results are presented on the durability of the polyimide Kapton H, which serves as a mechanically stable blanket material in solar arrays. To reduce degradation of this polymer from exposure to AO, it is typically coated with a thin layer of SiO_x where $1.9< x <2.0$. However, defects in the coatings exist which allow the base polymer to be attacked by energetic (4.5 eV) AO causing erosion of the polymer substrate with subsequent gradual loss in its mechanical integrity. Direct ground-test evaluation of the protective quality of coatings using an AO plasma is not simple due to differences in the AO flux directionality and energy distribution (~0.04 eV) compared with the in-space quantities. A Monte Carlo computer code

is being advanced which simulates AO reactions at defect boundaries. While this code has provided good results on erosion, its predictive capability is higher for directed atomic oxygen attack than isotropic plasma exposure.

To improve the Monte Carlo code, more faithful characterizations of AO reactions with polymers are needed which may be obtained through better understanding of undercutting at defect sites. Prior investigations (1-3) have yielded valuable information on cavity shape, size, and distribution. This information has guided revisions of the computational model concerning various AO interaction assumptions. A detailed list of the interaction parameters for Kapton used in the Monte Carlo code is given in reference (4).

The most prominent parameter affecting site-to-site variation in cavity evolution is the defect size. In general, and as expected, larger defects produce larger cavities. In addition, it has been observed (1) by examination of numerous defect sites that defect size is a factor in determining cavity shape. Other factors affect cavity shape and evolution. These factors may act independently or in concert in a complex fashion. For example, the present shape or size of a cavity may measurably affect its future evolution, leading to a non-uniform or nonlinear growth process. This may be the result of geometry, chemistry, transport phenomena or other physical phenomena.

Important aspects of cavity evolution can be studied without knowing the detailed nature of the erosion process. The effort of this study was directed toward capturing the gross trends in cavity evolution using simple models of cavity shape and fitting them to the measured diameters. The goal of the investigation was to determine whether cavity growth could be modeled adequately as a simple function of fluence or whether a more complex evolution model was needed. Such results will assist in understanding the undercutting process occurring with isotropic RF plasma asher exposures.

The following discussion involves the main rationale used in specifying cavity models. The first assumption is that a profile in the form of a simple arc, without inflexion points, can adequately approximate the true profile. The arc should be specifiable in terms of the upper and lower diameter measurements for undercut cavities that extend through the full thickness of the polymer. The second consideration is for specification during the period of evolution prior to the lower coating being reached. During this period, it is assumed that a cavity expands laterally at a rate approximating its vertical growth. Finally it is assumed that a cavity's profile retains a similar form throughout its evolution, so that a linear profile proceeds to evolve as a linear profile, even after reaching the lower coating, etc.

Three profile types were selected as models having the following forms: (1) linear arc, (2) parabolic arc and (3) circular arc. These arcs are used to generate a corresponding set of volumes of revolution used to model cavity growth. In terms of volume, linear and circular arcs produce values representing low and high bounds, respectively, with the parabolic profile producing values between these two. These profiles are discussed in detail.

2. MATERIAL CONSIDERATIONS

The polyimide Kapton is rapidly eroded by AO. An optically transparent coating, such as SiO_2, reduces erosion significantly. These coatings are very effective, even in layers typically no

thicker than 10-150 nanometers. However, small defects in the coatings, originating at application, permeate the protective layer and serve as sites for the AO to attack the exposed underlying Kapton. Although mechanically stable in its pristine form, its mechanical characteristics are compromised by chemical erosion. Significant erosion can make it unsuitable for its intended purpose.

3. EXPERIMENTAL

The study used a 13.56 MHz SPI Plasma Prep II operated with air. This type of asher produces plasma by the use of a low pressure, radio-frequency induced, gaseous discharge. The optical measurements were made using an Olympus Microscope. Coordinates were supplied using a xy-positioner.

The Kapton sample was cut from a sheet of 0.025-mm thickness Sheldahl-701664, covered on both faces with 0.13 microns (1300 Å) of SiO_x where $1.9<x<2.0$. The sample was mounted on a 2.5-cm by 7.5-cm slide and trimmed to this size. It was fastened by double adhesive tape along its periphery, designed to permit exposure to only the upper surface. During ashing sessions it was accompanied by a single 0.125-mm thick by 25-mm diameter witness coupon consisting of unprotected Kapton with only the upper face exposed to plasma. A fresh coupon was used for each session. Each witness coupon was weighed on a microbalance immediately before and after ashing sessions to determine its weight loss caused by erosion. The coupons were kept under vacuum prior to service to minimize moisture retention.

After ashing the sample for 66.5 hours, the sample was inspected and 27 defect sites were selected, with their positions relative to a corner being recorded. The sites were picked with emphasis on both shape circularity and the absence of nearby defects that might eventually grow into the selected site. As an aid to identification, sites were selected in sets of three, spaced apart by a few millimeters. The nine sets of sites were distributed more broadly about the entire untaped portion of the sample to provide diversity in location. The sites were inspected and measured after each session.

Effective cavity diameters were calculated by averaging the measurements of the silhouette obtained in two orthogonal directions lying in the plane of the sample. Figure 1 shows a digital image produced from an optical microscope photograph that reveals site 9. The black annular area, concentric with the site's center, corresponds to the sloped wall of the undercut cavity. Thus, the inner white portion represents the exposed silhouette of the lower protective coating. Similarly, the outer boundary of the black annular ring corresponds to the silhouette of the exposed upper coating where the defect is situated.

4. DISCUSSION OF RESULTS

Results were obtained at 27 protective coating sites on a single sample, with 26 sites surviving the entire ashing duration. One site became occluded by adjacent cavities after 610 hours of ashing and is thus excluded from duration-averaged statistics. The sample was ashed for

1306 hours over a period of two months consisting of 21 continuous ashing sessions spanning about two to three days each.

The effective fluence as determined by the witness-coupon mass lost through etching was essentially linear with ashing time over the period of investigation. The fluence versus ashing-time relationship is illustrated in Figure 2. A linear least squares regression through the origin gives a slope that establishes the ashing period of 1306 hours as being equivalent to a fluence of 1.96×10^{22} atoms /cm^2, yielding an average flux of 1.5×10^{19} atoms/cm^2-hr.

Cavity cross-sections were modeled using the three profile types with the assumption that the protective coating defects are very small compared to the overall thickness. The cavity cross-sections are illustrated by Figure 3(a) which corresponds to the case in which the cavity depth is less than the thickness of the sample and Figure 3(b) which corresponds to the case in which the cavity has reached the lower coating. In instances of the first case, the only measurable parameter is the upper diameter D equal to 2R. In instances of the second case the lower diameter d, equal to 2r, is also measured. In some instances of the second case, d is too small to be measured. As indicated in these figures, x denotes the lateral distance from the axis of rotation and z denotes the vertical distance from the cavity's bottom. Thus, the origin of the coordinate system is fixed to the bottom of the cavity, a distance h from the defect site. For all three models the profiles are specified in terms of the values of R and r measured at a given fluence, and the associated volumes of revolution are specified in terms of the corresponding diameters D and d.

It is assumed that the cavity depth h equals the upper radius R while it is growing, up to the instant it reaches the lower protective coating. This assumption is convenient and reasonably consistent with the data. The thickness of the Kapton is denoted by h_k. The profiles are presented in terms of the coordinates discussed above for the different degrees of evolution.

The expressions relating profile coordinates to the cavity parameters for the case $R < h_k$ are given by the Equations 1, 2, and 3 for the linear, parabolic and circular cases respectively.

$$z_{lin} = x, \qquad (0 \le x \le R < h_k) \qquad [1]$$

$$z_{par} = \frac{x^2}{R}, \qquad (0 \le x \le R < h_k) \qquad [2]$$

$$z_{cir} = R - \sqrt{R^2 - x^2}, \qquad (0 \le x \le R < h_k) \qquad [3]$$

The only parameter entering these relations is the upper radius R.

The volumes, V, of revolution corresponding to these profiles are those of a cone, paraboloid and hemisphere. These volumes are given, respectively, by Equations 4, 5 and 6.

$$V_{lin} = \frac{\pi}{24} D^3, \qquad (0 \le D < 2h_k) \qquad [4]$$

$$V_{par} = \frac{\pi}{16} D^3, \qquad (0 \le D < 2h_k) \qquad [5]$$

$$V_{cir} = \frac{\pi}{12} D^3, \qquad (0 \le D < 2h_k) \qquad [6]$$

The single parameter entering the volume expressions is D. From these relations it is readily observed that the volumes are in the ratio $V_{lin}:V_{par}:V_{cir} = 3:4:6$, for all $D < 2h_k$.

An analogous but somewhat more complex description is presented for the case $R \geq h_k$. For this case the expressions relating the three profiles to the parameters are given by Equations 7, 8 and 9 for the linear, parabolic and circular arc profiles, respectively.

$$z_{lin} = \frac{h_k}{R-r}(x-r), \qquad (r \leq x \leq R),\ (R \geq h_k) \qquad [7]$$

$$z_{par} = \frac{h_k}{(R-r)^2}(x-r)^2, \qquad (r \leq x \leq R),\ (R \geq h_k) \qquad [8]$$

$$z_{cir} = z_c \pm \sqrt{R_c^2 - (x-x_c)^2}, \qquad (r \leq x \leq R),\ (R \geq h_k) \qquad [9]$$

The additional parameter r explicitly occurs in the expressions for the linear and parabolic profiles and implicitly enters in the case of the circular arc. For the linear and parabolic cases, the profile shapes are similar to their respective shapes for the case R less than h_k, with simple scaling and translation transformations being introduced. For the case of the circular arc the explanation is more involved.

A hemispherical arc is too restrictive, and a general circular arc is sought allowing for a radius of curvature different from R, denoted by R_c. For a circular arc to serve as a suitable profile, it must meet the lower surface at the measured distance r from the axis and meet the upper surface at the measured distance R from the axis. A truncated hemispherical profile of radius R is not suitable since, in general, it would not join the lower surface at the measured r. The specification of a general arc of radius R_c is partially determined by the measured values of R and r. For any circular arc passing through two specified points, its center must be on the perpendicular bisector of the two points. The freedom to choose a center among the points on this line exists. Once the center of the arc is determined, R_c is likewise determined since it must pass through the upper and lower surface points. Designate the coordinates of the center of the arc as $x = x_c$, $z = z_c$.

To give us a basis for determining a unique value for R_c, the equation for the volume of a truncated hemisphere of thickness h_k is examined. The volume V_{hem} of a truncated hemisphere of thickness h_k and diameter D is given by Equation 10.

$$V_{hem} = \frac{\pi h_k}{12}\left(3D^2 - 4h_k^2\right) \qquad [10]$$

This volume can be expressed in terms of D and d_{hem} as given by Equation 11.

$$V_{hem} = \frac{\pi h_k}{12}\left(2D^2 + d_{hem}^2\right) \qquad [11]$$

The value of d_{hem} is set by Equation 12.

$$d_{hem} = \sqrt{D^2 - 4h_k^2} \qquad [12]$$

Equation 11 is also valid for volumes V_{cir} generated by circular arcs obtained when general d, not restricted by Equation 12, are substituted for d_{hem}. For the case of d satisfying the range given by $0 < d < d_{hem}$, the volumes are such that $V_{cir} < V_{hem}$; for the case of d in the range $d_{hem} < d < D$, the volumes reverse order such that $V_{cir} > V_{hem}$. Thus, we establish a unique volume corresponding to our measured values D and d. To obtain the profile for this arc, its radius R_c is needed. This value is determined through an iteration process.

The iteration begins by selecting a preliminary value of R_c. Next, values for x_c and z_c are obtained that are consistent with the equation for a circle given by Equation 9, for x = r and x = R. This establishes a preliminary arc. The volume contained by the surface of revolution is calculated numerically and compared to the value V_{cir} obtained from Equation 11 using the measured d in place of d_{hem}. If the values agree within some specified tolerance, the arc is acceptable, otherwise, the iteration cycle is repeated, starting with a new value for R_c.

Equations 13, 14 and 15 give the volumes for the linear, parabolic and circular arc profiles just discussed for the case $R \geq h_k$.

$$V_{lin} = \frac{\pi h_k}{12}\left(D^2 + Dd + d^2\right), \qquad (D \geq 2h_k) \qquad [13]$$

$$V_{par} = \frac{\pi h_k}{24(D-d)^2}\left(3D^4 - 4D^3 d + d^4\right), \qquad (D \geq 2h_k) \qquad [14]$$

$$V_{cir} = \frac{\pi h_k}{12}\left(2D^2 + d^2\right), \qquad (D \geq 2h_k) \qquad [15]$$

The two parameters D and d determine the volume for the three profile types. However, there is one more situation involving cavity evolution that must be considered. This situation exists when the cavity has reached the lower coating but the lower cavity diameter d is too small to be measured. In this instance for the case $R \geq h_k$, Equation 16 is used for either a linear or parabolic profile, or Equation 12 for a circular arc profile to provide a value for d as required in the Equations 13, 14 and 15.

$$d = D - 2h_k \qquad [16]$$

Similarly, r as determined by the appropriate Equation 12 or 16 is substituted in the Equations 7, 8 and 9 for the profiles. The effect of the above is to smoothly extend the profile description for the case R less than h_k to cover the transition zone, where R is greater than h_k but d is not measured. The profiles and volumes for this transition zone are expressed by the following equations:

$$z_{lin} = x + h_k - R, \qquad (R - h_k \leq x \leq R), (R \geq h_k) \qquad [17]$$

$$z_{par} = \frac{1}{h_k}(x + h_k - R)^2, \qquad (R - h_k \leq x \leq R), (R \geq h_k) \qquad [18]$$

$$z_{cir} = h_k - \sqrt{R^2 - x^2}, \qquad (R - h_k \leq x \leq R), (R \geq h_k) \qquad [19]$$

$$V_{lin} = \frac{\pi h_k}{12}\left(3D^2 - 6Dh_k + 4h_k^2\right), \qquad (D \geq 2h_k) \qquad [20]$$

$$V_{par} = \frac{\pi h_k}{12}\left(3D^2 - 4Dh_k + 2h_k^2\right), \qquad (D \geq 2h_k) \qquad [21]$$

$$V_{cir} = \frac{\pi h_k}{12}\left(3D^2 - 4h_k^2\right). \qquad (D \geq 2h_k) \qquad [22]$$

As can be seen, the only measured parameter is R or D in Equations 17 through 22.

Individual results are given in the light of mean results. The mean upper diameter, as averaged over all cavity sites, was found to be 0.015 mm at the end of the first ashing period, growing to a mean upper diameter of 0.069 mm by the end of the final ashing. Figure 4 shows the evolution, denoted by the open diamond symbol, of the mean upper diameter with effective fluence. The diameter is expressed directly in mm on the primary dependent axis and expressed in normalized form as a ratio with h_k on a secondary axis. A single-term power curve, illustrated by the solid line in this figure, approximates the data quite well as represented by the following function of fluence

$$\overline{D} = cF^n . \qquad [23]$$

Here, $\overline{D}$ represents the mean upper diameter, expressed in mm, c is a numerical coefficient depending on employed units, n is a real-valued exponent and F is the fluence (atoms/cm^2). The exponent value obtained by regression is n = 0.51. The advantage of the single-term power curve over a polynomial curve lies in its interpretive quality, not in its predictive quality. For instance, the value of the exponent n gives a good measure of the degree of linearity in the data. For a polynomial, this judgement might be hard to reach by just looking at the formula.

The form of diameter growth as given by Equation 23 also gives a very satisfactory description of the evolution of individual sites. The evolution of D is shown in Figure 5 for a representative group of sites. As indicated by the curves, the growth of D is less than linear. The volume evolution cannot be determined from these curves alone. This is because the lower diameter begins to evolve at values of D approximately equal to $2h_k$. An example is presented in Figure 6 for site 1 illustrating the onset of measurable d. This figure includes evolution of the cavity's lower diameter as well as its upper diameter. The value of the exponent returned by regression for the upper diameter is n = 0.61 for site 1. The lower diameter is also adequately represented in a form similar to Equation 23, but with fluence adjusted by a constant term representing the amount of fluence, F_o, required for the lower diameter to begin evolving. The corresponding form of evolution of the lower diameter, d, is given by

$$d = c\left(F - F_o\right)^n . \qquad [24]$$

The regression value for the lower diameter's exponent is n = 0.65, with F_o = 5.4 for this site. The value assigned to F_o is determined by iteration, based on a measure of correlation with the data. For this example, the exponent n obtains a higher value for the lower-diameter curve than for the upper-diameter curve, indicative that the lower diameter is expanding at a higher rate than the upper one. This result held for all other sites that grew to reach the lower coating. This evolvement is as expected if one believes, for example, that cavity shape tends to the shape of a cylinder at very large diameter. Figure 7 shows the profile of the circular-arc model at various stages in the evolution of site 1. In Figure 8 profiles for the three model types are shown pertaining to three stages of evolution for this site. As the evolution proceeds, the

parabolic-arc profile expands laterally at the cavity's lower region at a faster rate than the other two profiles. For the last two stages shown, it extends beyond the circular-arc's profile near the lower coating, while remaining within the circular-arc's profile near the upper coating.

The extent cavity walls become steeper can be seen by plotting the difference between the measured upper and lower radii, R-r, over the evolution period. It is convenient to present results in terms of Kapton thickness where distance is normalized by h_k. Figure 9 shows the radius-difference-to-Kapton-thickness ratio as a function of the upper-radius-to-Kapton-thickness ratio for all the appropriate sites. The measured data are presented as open diamonds. The solid curve, which begins at a ratio of one and decreases monotonically, describes the curve corresponding to a hemispherical profile shape. The dotted curve represents a model approximating the variation of radius difference. The initial section of the plot, R/h_k less than one, is the region where the lower boundary has not been reached, and wall slopes are indeterminate. Consequently, with r defined as zero in this region, the data vary directly with R. As growth continues, the radius-difference-to-thickness ratio continues to increase, until r becomes measurable and increases faster than R, at which point the measured radius difference decreases abruptly. This change is seen to occur at values of R/h_k slightly greater than one. For values of R/h_k of about 1.25 and greater, the radius difference remains nearly constant, such that the radius-difference-to-thickness ratio, $(R-r)/h_k$, is about 0.75. Thus, at large R-values the cavity wall appears to erode laterally with constant mean slope, $h_k/(R-r)$, approximately equal to 1.3. It is clear that a hemispherical profile produces a wall too steep to adequately match the data for radius-to-thickness ratios greater than about 1.5. A more realistic description of the variation of radius gap is given by the dotted curve. The initial point for the slanted portion of the dotted curve corresponds to a value of one for both r and R. This positioning of the curve is conservative on the low side, and a positioning of as much as 10 percent higher seems justifiable.

It is reasonable to conclude from the above that a cavity expands as fast or somewhat faster laterally, at least near the upper coating, than it expands vertically. The abrupt decline in radius gap at radius-to-thickness ratios near 1.25 may be due to an erosion process whereby a thin layer of polymer adjacent to the lower coating is removed fairly rapidly, accelerating the increase in r compared to the increase in R occurring at the upper coating. Once this thin crust is depleted, the cavity expands laterally with erosion distributed uniformly along the wall.

As given above, the equations for the profiles and volumes have different forms for the case R less than h_k as compared to the case where R is greater than or equal to h_k. It is reasonable to examine how this difference is manifested in terms of curve fitting. From the example of site 1 given in Figure 6, it appears that D increases fairly smoothly with fluence as evidenced by the comparison to the fitted regression line. However, we can consider the upper curve as two sections joined at R/h_k equal to one, roughly at F_o=5.4. Motivated by the knowledge that the functional form of the profile changes, the upper curve is fitted by regression separately for the two sections. Sectionalized regression of the upper-diameter evolution of site 4 is illustrated in Figure 10, where the dotted lines represent the regression curves for each upper-diameter section. The evolution of d is also included, represented by solid symbols. For this site, regression gives n=0.53 for the lower fluence section and n=0.66 for the higher fluence section. For the six largest sites, the average difference in values of n between the two upper sections is 0.15, with the higher value obtained for the higher fluence section. This observed change in the exponent value at R=1 is consistent with the model equations for cases where volume evolves smoothly with respect to fluence.

By examining Equations 6 and 15 for the circular model, it is seen that D varies as the one-third power of the volume for R less than h_k and as the one-half power for R much greater than h_k. The latter result represents the variation of the diameter of a cylinder as a function of its volume. It can be derived formally from the model equations by obtaining the limiting form of V as a function of D as d approaches D, and then expressing D in terms of V. For a volume evolution in which V varies as a constant power of F, it follows that D, when expressed by Equation 23, has a larger exponent value for the higher fluence section as compared to the value for the lower fluence section. However, the exact increase in n as R increases is complicated by terms containing d whose precise variation is unknown.

To examine the volume evolution, the volume is described as a function of fluence in a form given by Equation 25, which is of the same form as Equation 23.

$$V = bF^m \qquad [25]$$

This form was fitted by regression using values of volume obtained from the geometric models. The regression was performed after transforming Equation 25 into the linear form given by Equation 26.

$$V^{1/m} = b^{1/m}F \qquad [26]$$

The exponent values, m, which differ according to site, were determined by iteration. Figure 11 shows a comparison between the measured volume evolution and predicted volume evolution for several sites using the circular-arc profile model. The volume is expressed in dimensional units on the primary dependent axis, and expressed as a ratio given by the site-volume-to-unit-hemisphere-volume, where the unit-hemisphere's radius equals h_k, on a secondary axis. For instance, using the secondary measure, a hemispherical cavity of radius h_k has a volume ratio of one. It can be seen from the figure that the final volume for the largest site shown is approximately 9 unit-hemispheres. The sites maintain a constant relative volume ranking with fluence. It was found that the evolution of all sites is represented very satisfactorily by an equation of the form given by Equation 25. In general, the regression exponent for the power-law curves increases with increasing value of the final volume. To give a representation of this variation, the site-distribution of m is presented as a function of the final site volume in Figure 12. In this figure m is shown as a function of the final-site-volume-to-average-final-site-volume ratio using a log scale. The average final site volume is 1.0×10^{-4} mm^3 (3.0 unit hemisphere) and the largest site volume measured is 5.9×10^{-4} mm^3 (17.2 unit hemisphere).

Use of the linear and parabolic models produced similar evolution results as compared to the circular-arc profile case. Figure 13 shows comparisons between the predicted volume evolution for all three models for selected sites. The predicted volume for the parabolic model remains between the volume of the linear model and the volume of the circular-arc model at all fluence levels. For larger cavities, the difference in volume between the parabolic and circular-arc cases is very slight at higher fluence levels, whereas, the difference in volume between the linear and circular-arc volumes remains relatively constant. For smaller sites the three models give the same values of m. For larger sites, the linear and parabolic models produce evolutions resulting in somewhat higher values of exponent m compared to the circular-arc model. This is because the volume ratios for the linear, parabolic and circular-arc models start at 3:4:6, respectively, and approach one at higher fluence. This geometric effect accordingly determines

the volume evolution for the three models. Compared to the circular-arc model, the other two models lag early, then play "catch-up" later.

5. SUMMARY AND CONCLUSIONS

Cavity evolution occurring in protected Kapton, exposed to an effective fluence of about $2x10^{22}$ atoms/cm^2 in a plasma asher, was investigated. The growth of numerous cavities occurring underneath pin-window defects in the exposed upper protective coating was monitored by recording cavity diameters using microscopy. Three geometric models were used to estimate cavity volume. These models calculate volumes based on cavity diameters measured adjacent to the upper protective coating and the lower coating.

Cavity diameters were seen to vary smoothly, but less than linearly, as a function of fluence. The evolution of the upper and lower diameters can be fitted satisfactorily by a set of simple fluence power-law curves. For large cavities the upper diameter was split into two sections for regression, corresponding to the associated variation in the geometric model with cavity diameter. The exponent obtained for the larger diameter section is generally greater than that of the smaller diameter section. It was found that a typical wall for a large cavity has a slope that is approximately 1.3. The corresponding site volumes were seen to evolve smoothly with fluence. It was found that site volume is fitted satisfactorily using simple fluence power-law curves. The sites maintained their volume ranking. Sites that were initially small compared to the average site remained relatively small as they evolved, etc. The volumes of the smaller-volume sites increased less than linearly, whereas, the volumes of larger-volume sites increased greater than linearly with fluence.

6. REFERENCES

1. B. A. Banks, B. M. Auer, S. K. Rutledge, and C. M. Hill, "Atomic Interaction with Solar Array Blankets at Protective Coating Defect Sites," presented at the 4th Annual Workshop on Space Operations, Automation and Robotics (SOAR 90), NM, June 1990.
2. B. A. Banks, S. K. Rutledge, K. K. de Groh, B. M. Auer, and C. M. Hill "Atomic Oxygen Protective Coatings," presented at the NATO Advanced Study Institute Conference, Pitlochry, Scotland, July 1991.
3. B. A. Banks, K. K. de Groh, S. K. Rutledge, and F. DiFilippo, "Prediction of In-space Durability of Protected Polymers Based on Ground Laboratory Energy Atomic Oxygen," NASA Technical Memorandum TM 107209, 1996.
4. B. A. Banks, T. J. Stueber, S. A. Snyder, S. K. Rutledge, and M. J. Norris, "Atomic Oxygen Erosion Phenomena," presented at the American Institute of Aeronautics and Astronautics Defense and Space Programs Conference, Alabama, September 1997.

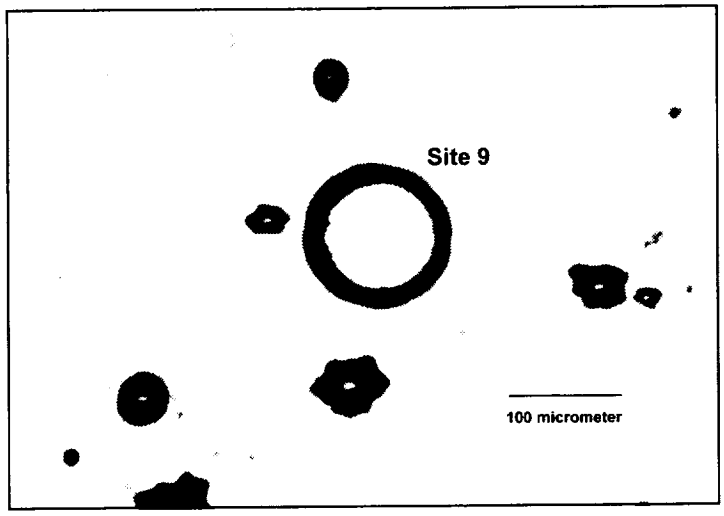

Figure 1. Image of concentric silhouettes of site 9.

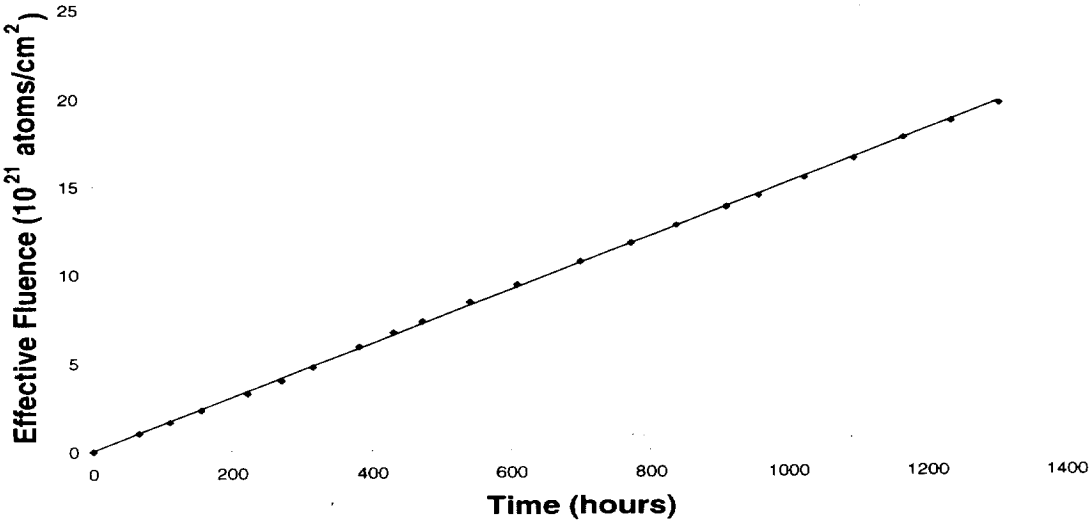

Figure 2. Effective fluence dependence on ashing time.

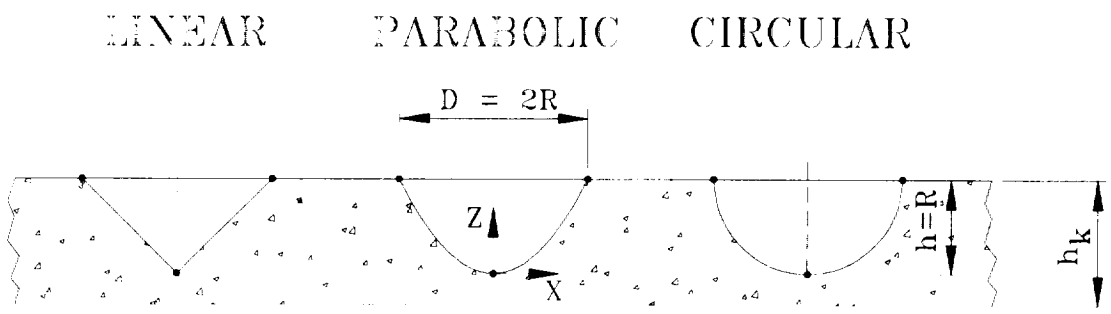

(a)

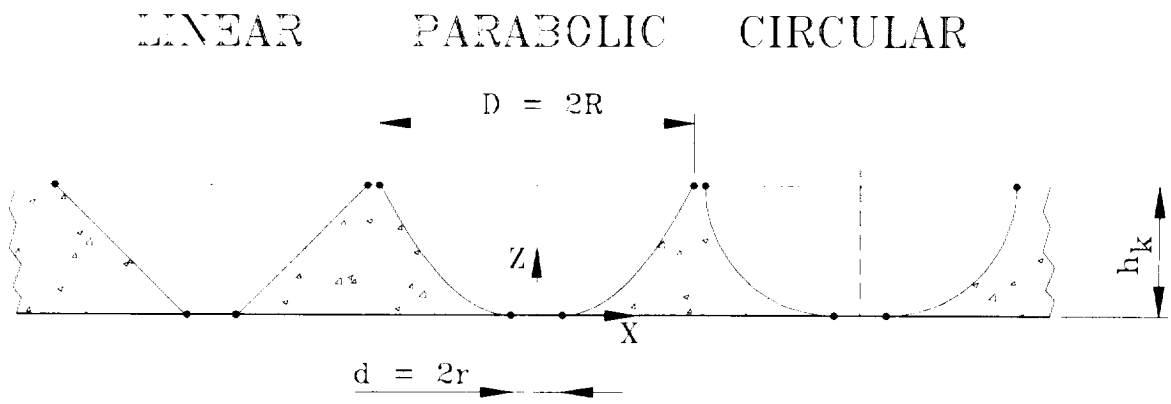

(b)

Figure 3. Illustration of the three profile models and the coordinate systems used for the two evolution regimes: (a) $R<h_k$ and (b) $R \geq h_k$.

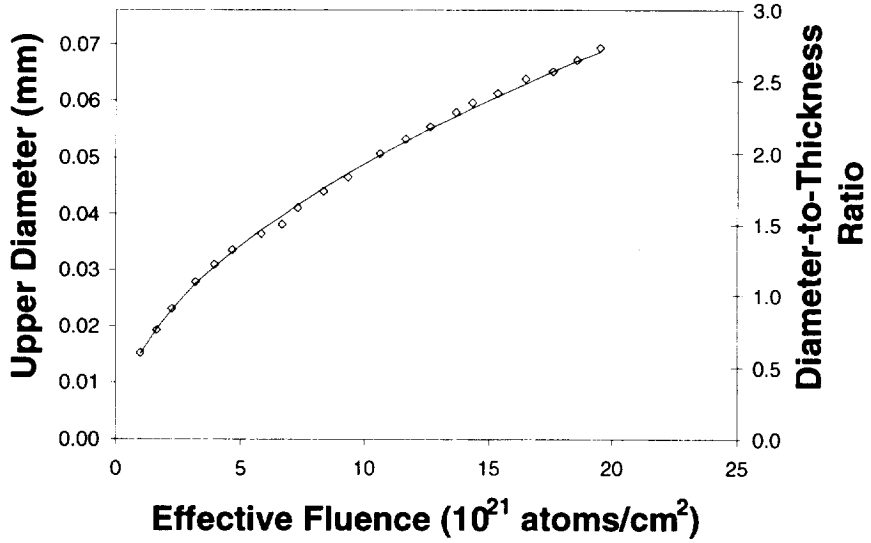

Figure 4. Evolution of mean cavity upper diameter with fluence.

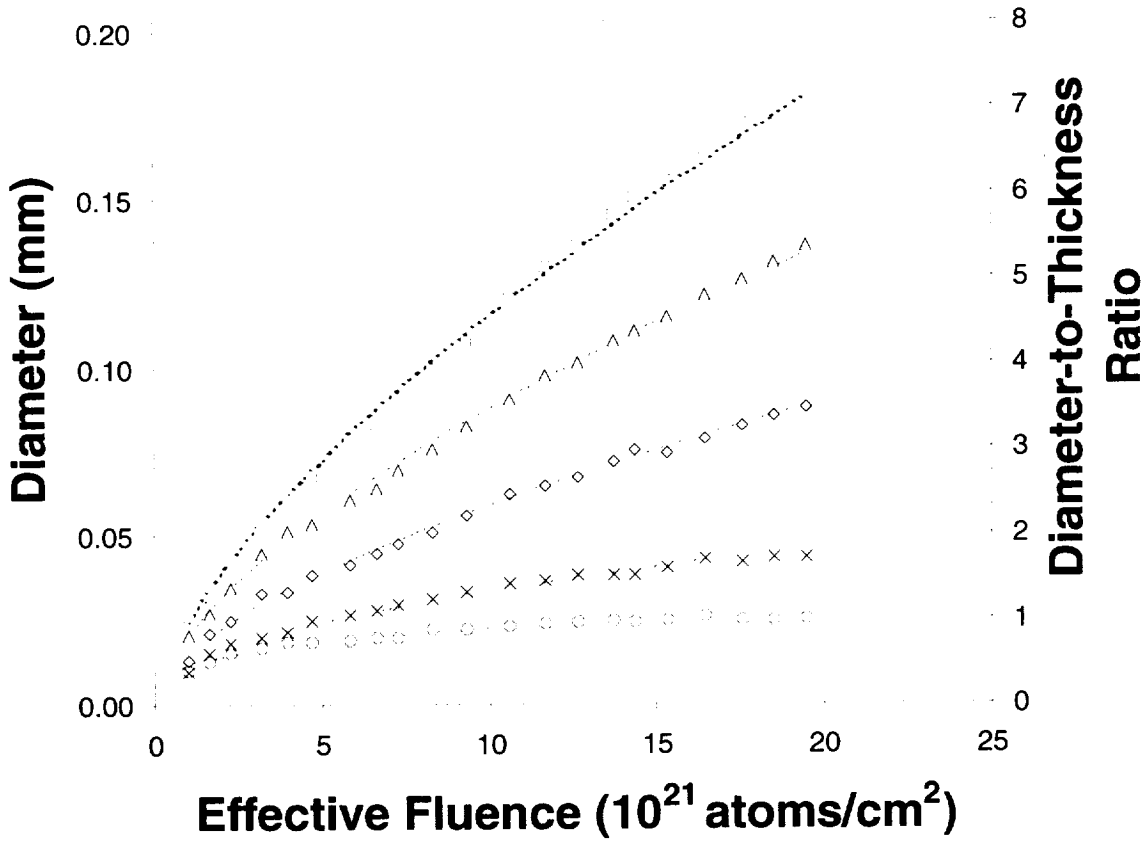

Figure 5. Evolution of cavity upper diameter with fluence for representative sites.

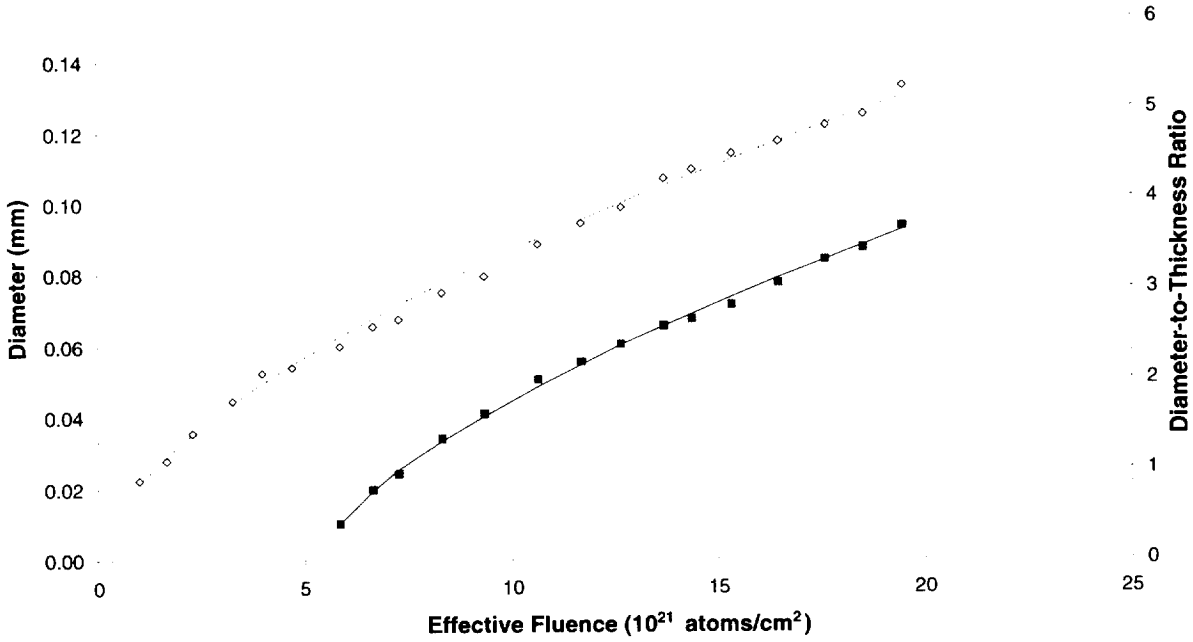

Figure 6. Evolution of lower (solid) and upper (open) diameters with fluence for site 1.

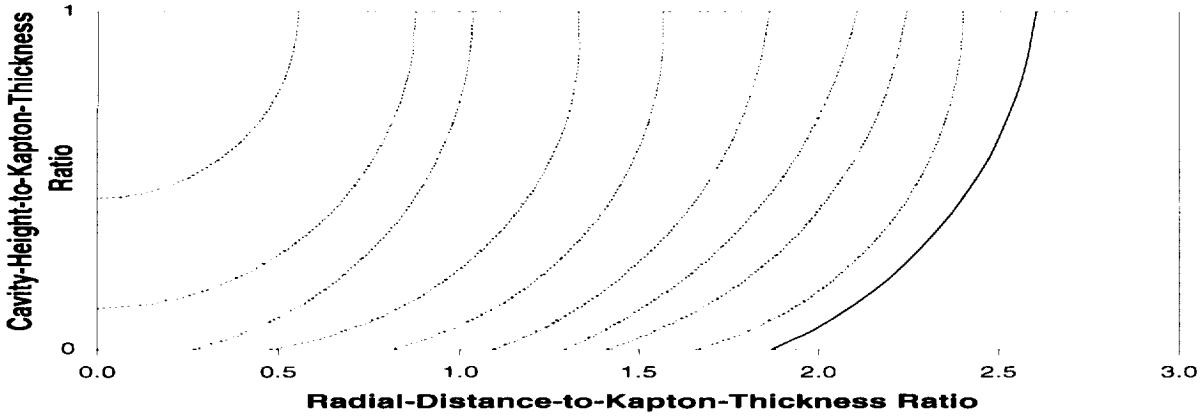

Figure 7. Circular-arc profiles at various stages of evolution for site 1.

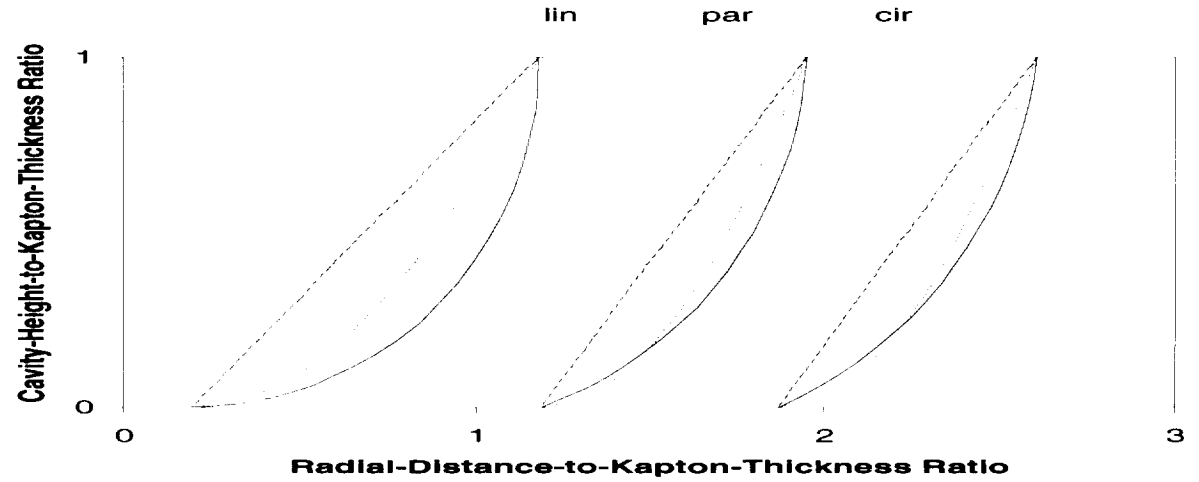

Figure 8. Comparison of the profile models at three stages of evolution for site 1.

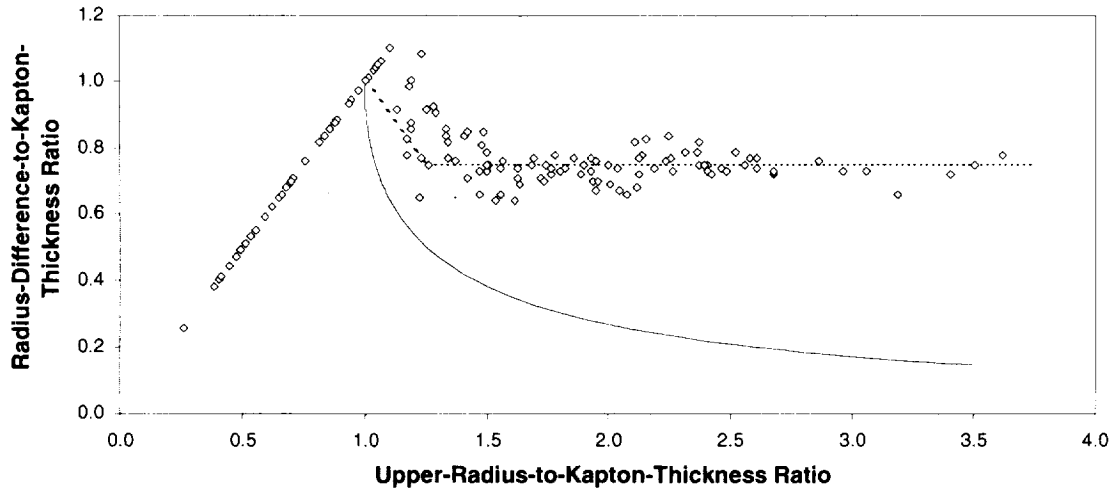

Figure 9. Radius difference dependence upon upper diameter for the following: (1) data (open diamond), (2) truncated hemisphere (line), and (3) reasonable model (dotted).

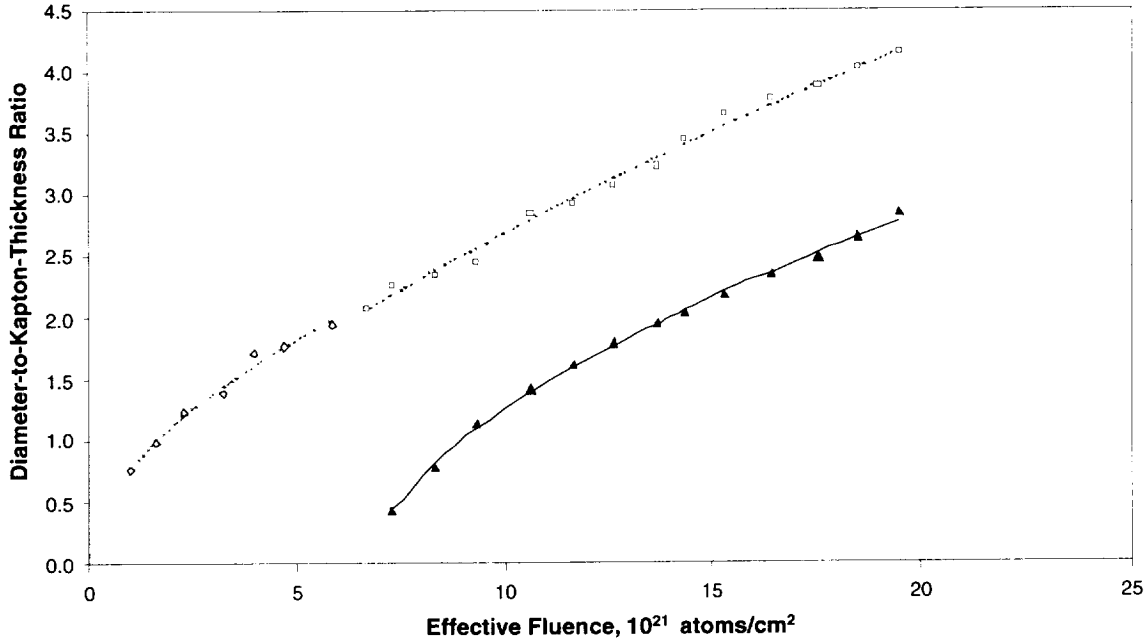

Figure 10. Evolution of upper (open) and lower (solid) cavity diameters for site 4 with fluence, showing for comparison the sectionalized regression curves (dotted) of upper diameter growth and the regression curve (solid) for lower diameter growth.

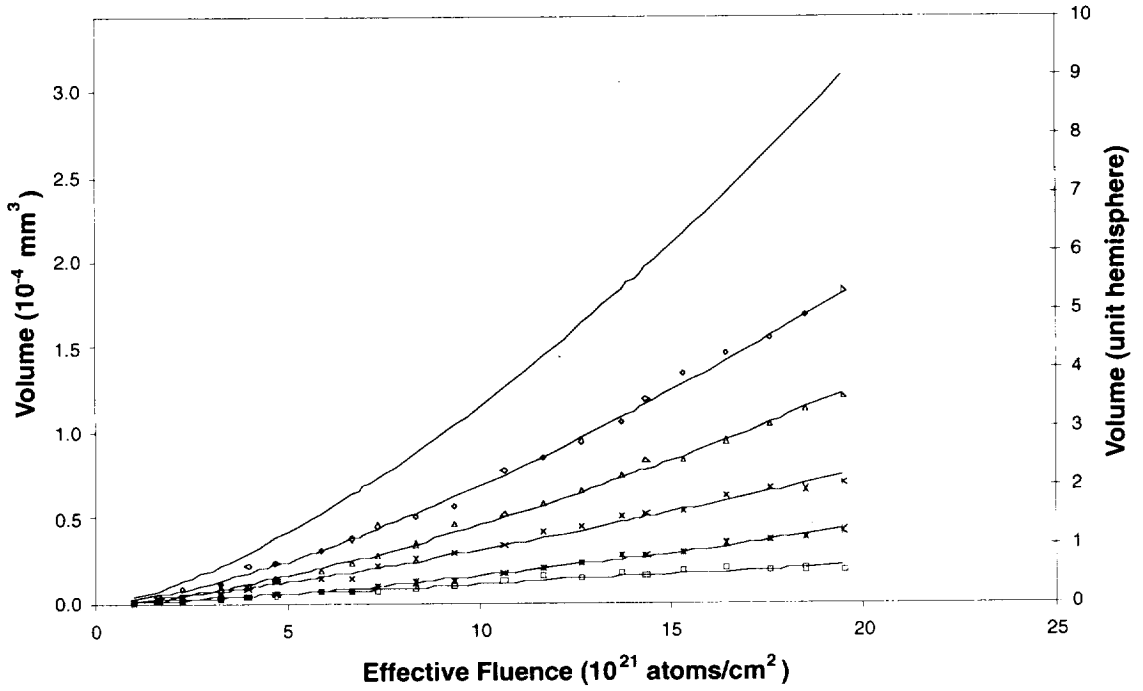

Figure 11. Comparison of the dependence of measured volume evolution (open symbols) upon fluence using the circular-arc model with the dependence of power-law volume evolution (solid curves) upon fluence for representative sites.

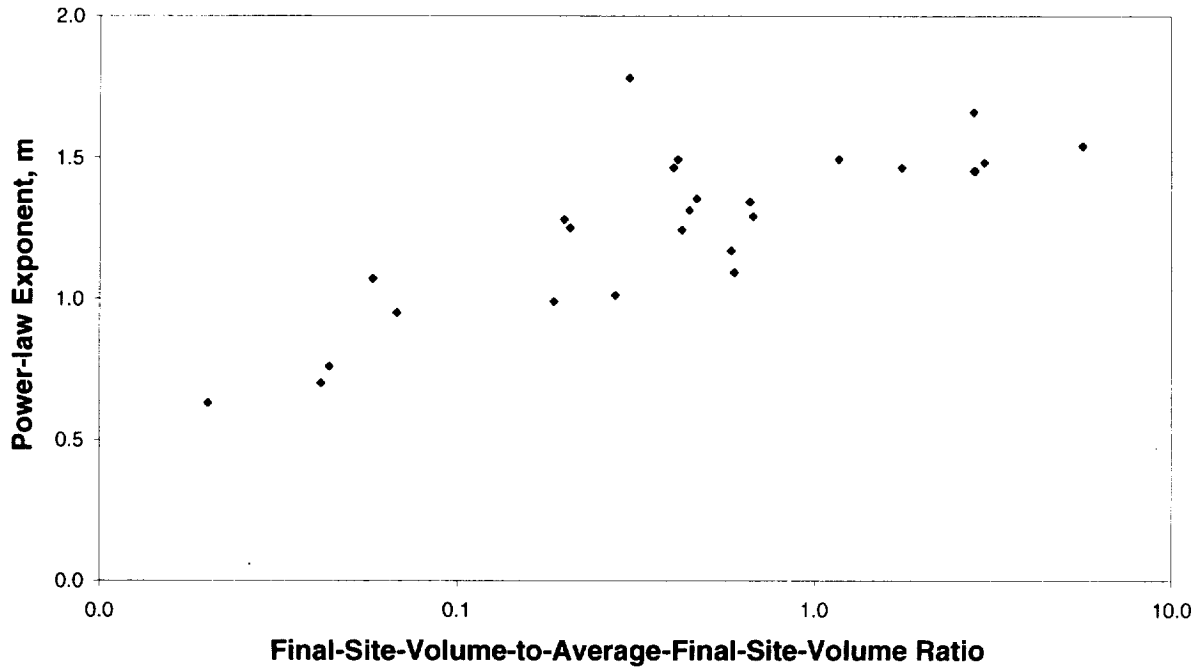

Figure 12. Dependence of the power-law exponent, m, upon final relative cavity volume.

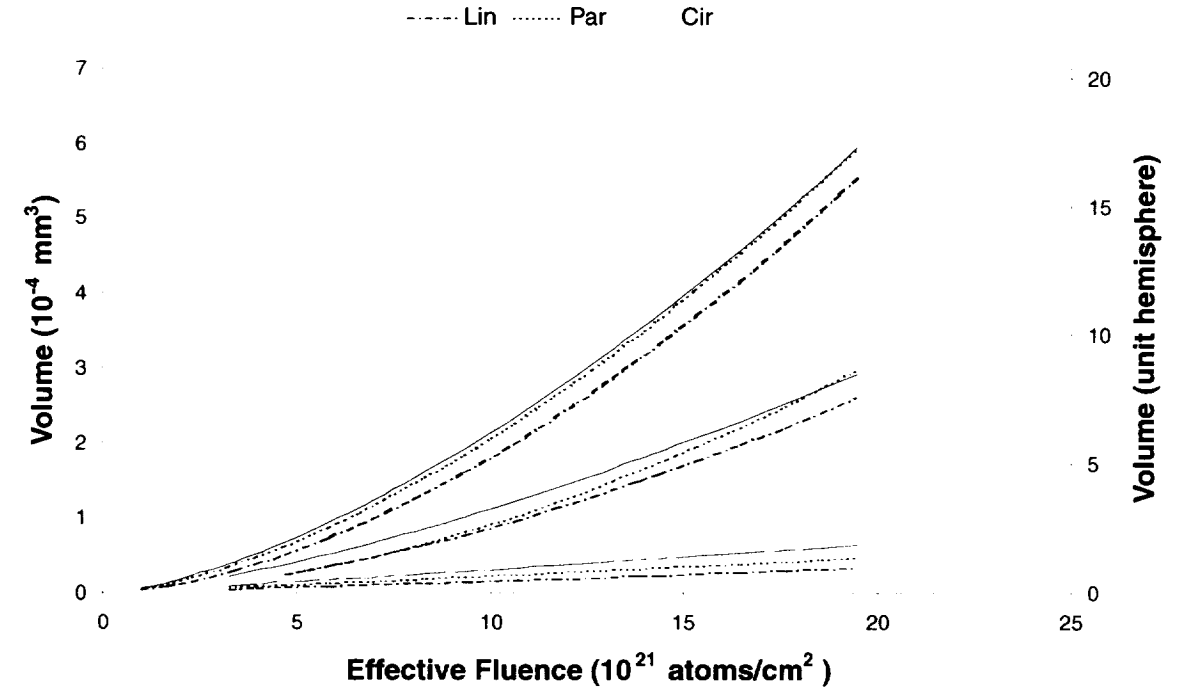

Figure 13. Comparison of power-law volume evolution with fluence among the three model types: linear (broken), parabolic (dotted), and circular (solid) for representative sites.

REPORT DOCUMENTATION PAGE

Form Approved
OMB No. 0704-0188

1. AGENCY USE ONLY (*Leave blank*)	2. REPORT DATE	3. REPORT TYPE AND DATES COVERED
	May 1999	Technical Memorandum

4. TITLE AND SUBTITLE

Investigation Of Atomic Oxygen Erosion Of Polyimide Kapton H Exposed To A Plasma Asher Environment

5. FUNDING NUMBERS

WU-632-1A-1E-00

6. AUTHOR(S)

Aaron Snyder

7. PERFORMING ORGANIZATION NAME(S) AND ADDRESS(ES)

National Aeronautics and Space Administration
John H. Glenn Research Center at Lewis Field
Cleveland, Ohio 44135-3191

8. PERFORMING ORGANIZATION REPORT NUMBER

E-11687

9. SPONSORING/MONITORING AGENCY NAME(S) AND ADDRESS(ES)

National Aeronautics and Space Administration
Washington, DC 20546-0001

10. SPONSORING/MONITORING AGENCY REPORT NUMBER

NASA TM—1999-209178

11. SUPPLEMENTARY NOTES

Prepared for the 44th International SAMPE Symposium and Exhibit sponsored by the Society for the Advancement of Material and Process Engineering, Long Beach, California, May 23–27, 1999. Responsible person, Aaron Snyder, organization code 5480, (216) 433–5918.

12a. DISTRIBUTION/AVAILABILITY STATEMENT

Unclassified - Unlimited
Subject Categories: 27 and 18 Distribution: Nonstandard

This publication is available from the NASA Center for AeroSpace Information, (301) 621-0390.

12b. DISTRIBUTION CODE

13. ABSTRACT (*Maximum 200 words*)

Experimental results are presented on the erosion characteristics of the polyimide Kapton H, which serves as a blanket material in solar arrays. This polymer has a number of characteristics that make it a suitable choice for both terrestrial and space applications. In this paper attention is focused on the durability of protected Kapton when exposed to atomic oxygen (AO) in a plasma asher. A strip of 0.025-mm thick Kapton film, coated on both sides with SiO_2, was studied during a 1306 hour exposure. The erosion, located at defect sites in the protective coating and measured optically, is described in terms of volume loss as a function of AO fluence. Three simple geometric profiles are used to generate a useful array of cavity shapes to model erosion evolution. These models connect the volume erosion rate to the observed lateral expansion of the developing cavities via their diameters, measured adjacent to the upper and lower protective film, and fitted by least-squares regression to simple power law functions of fluence. The rationale for the choice of models is discussed. It was found that lateral growth in cavity size evolves less than linearly with fluence.

14. SUBJECT TERMS	15. NUMBER OF PAGES
Oxygen atoms; Protective Coatings; Erosion	22
	16. PRICE CODE: A03

17. SECURITY CLASSIFICATION OF REPORT	18. SECURITY CLASSIFICATION OF THIS PAGE	19. SECURITY CLASSIFICATION OF ABSTRACT	20. LIMITATION OF ABSTRACT
Unclassified	Unclassified	Unclassified	